DOI: https://doi.org/10.24297/jap.v16i1.8362

Optical And Electrical Properties of PVA/α-Al_2O_3 Nanocomposite Films

A. F. Mansour[1], Sara El-Molla[1,2*], R. Mamdouh[1] and M. A. Abdo[1]

[1]Physics Department, Faculty of Science, Zagazig University, Egypt

[2]College of Engineering, University of Business and Technology (UBT), Jeddah, Saudia Arabia

*elmolla4science@yahoo.com, elmolla4science@zu.edu.eg

Abstract

In the present study, α-Al_2O_3 nanoparticles were synthesized using the citrate-nitrate auto combustion method. Nanocomposites of PVA/α-Al2O3 were intended by solution casting technique. The micrograph of samples were analysed by X-ray diffraction (XRD), high resolution transmission electron microscopy (HRTEM), field emission scanning electron microscopy (FESEM) and UV-visible spectroscopy analysis. UV-visible results showed that the direct optical band gap decreased with the increase of α-Al_2O_3 content. The refractive index has been dissected using Wemple and DiDomenico model. Hopping of charge carriers besides interfacial polarization could expound the demeanor of dielectric constant (ε'), dielectric loss (ε'') and ac electrical conductivity (σac) with the frequency and temperatures.

Keywords: PVA;A α-Al_2O_3 nanoparticles; Nano composites; optical constants; electrical properties.

1. Introduction

Nanoparticles' research is presently an objective domain of scientific weal due to its potential applications in several fields from optical, electrical to biological. Metal oxide nanoparticles have been exceedingly improved in the past decennium. They have been vastly utilized in numerous applications such as catalysts, sensors, semiconductors, medical science, capacitors, and batteries [1–6]. Among them, aluminum oxide, Al_2O_3, is transpiring . Alumina has sundry phases such as gamma , delta , theta , and alpha , the farthest thermodynamically stable form is α-Al_2O_3 [7]. Al_2O_3 have become more prevalent for their high dielectric strength, a wide optical
band gap, exceptional stability, and durability against hostile environments and high transparency down to 250 nm. Also, α-Al_2O_3 been excessively utilized for their practical applications, such as refractory coatings, antireflection coatings, anticorrosive coatings [8], microelectronic devices [9], capacitance humidity sensors [10], and silicon solar cells [11], and as insulating material, in the form of thin films, in semiconductor devices [12]. Polymer nanocomposites have received intensive awareness and research in the neoteric years. Polymer nanocomposites have been elaborated for their marvelous properties such as light weight, high flexibility, and ability to be feigned at low temperature and low cost, and application in various fields such as radiation detection, coating, paints, sensors, LEDs, display, optoelectronics devices and biological application [13-16]. The physical properties of polymers may be influenced by doping α-Al_2O_3. Polyvinyl alcohol (PVA) is a semi crystalline, non-toxic, water soluble and mild electrical conductivity material with numerous technological and biomedical applications [17]. In this work, synthesis and characterization of α-Al_2O_3 nanoparticles then preparing PVA/α-Al_2O_3 nanocomposite films via dispersion different amount of the α-Al_2O_3 (0, 2.5,5,7.5, 10, and 15 wt%) in PVA matrix were investigated. The resulting hybrid films were described by X-ray diffraction (XRD), Fourier transform infrared spectroscopy (FT-IR), field emission scanning electron microscopy (FE-SEM), and UV-visible absorption spectra techniques, then optical and electrical properties were studied.

2. Materials and Methods

Polyvinyl alcohol (PVA) from Sigma Aldrich, with average molecular weight of 50,000–85,000 and 97% hydrolyzed was used without further purification. Aluminum nitrate [Al $(NO_3)_3.9H_2O$] and citric acid ($C_6H_8O_7$)

also were purchased from Aldrich. Reactant solutions were made in doubly distilled water. Nano-sized particles of α-Al_2O_3 were prepared using the citrate-nitrate combustion method [18]. The molar ratio of metal nitrates to citric acid was 1:1. A small amount of ammonia was added to the solution to adjust the pH value at 7. The precursor mixture was then heated to 1200˚C for 5h. The nanocomposite films were prepared by the well-known solution casting technique. The as prepared α-Al_2O_3 nano powders was added into the aqueous solution of PVA in the following composition (w/w between α-Al_2O_3 and PVA solution concentration): 0%, 2.5%, 5%, 7.5%, 10% and 15% then stirred carefully by using magnetic stirrer until well dispersion α-Al_2O_3 / PVA was obtained. Each mixture is put in a Petri dish and leave to dry in a dust free chamber at room temperature to obtain the nanocomposite films. The X-ray diffraction (XRD) patterns were recorded at room temperature using an X-ray powder diffractometer (Shimadzu XRD 6000) equipped with CuK_α as radiation source (λ = 1.54Å.) in the 2θ (Bragg angles) range ($10^\circ \leq 2\theta \leq 80^\circ$) to report the information about their structure. The morphology and particle size distribution of the samples were identified using high resolution transmission electron microscope (HRTEM) JEOL-2100 at 200 KV. The Fourier transform infrared (FTIR) Jasco (Model 6100, Japan) was used in the range 400– 4000 cm^{-1} and in the absorbance mode at a resolution of 4.0 cm^{-1}. The morphology of the samples was identified using the field emission scanning electron microscope (FESEM) model Quanta FEG250. Different phases were conducted by Energy Dispersive X-ray Spectrometry (EDS). The absorbance spectra (A) and the transmittance spectra (T) of the films were recorded at 200–1100 nm wavelength using a dual beam (UVS-2800) UV–Visible spectrophotometer. The dielectric measurements were measured using impedance analyzer (IM3570) in the temperature range from 303 to 453 K in the frequency range from 4 Hz to 5 MHz.

3. Results and Discussion

3.1. X-ray analysis

The X-ray diffraction pattern (XRD) for pure polyvinyl alcohol (PVA) sample is shown in Fig.1a. The XRD pattern manifests a strong broad diffraction peak appeared at 2Θ= 20.12° which identical to (101) reflection plane of PVA and a more peak at 41.62°; confirming the semi-crystalline nature of PVA i.e., entity of crystalline and amorphous parts [19-20]. This diffraction peak assured that, the PVA film is pure without any other impurities. Fig.1b shows the XRD of highly crystalline α-Al_2O_3. The crystal planes, (012), (104), (110), (006), (113), (024), (116), (211), (018), (214) and (300) confirmed the formation of α–Al_2O_3 in a pure single hexagonal phase according to JCPDS card no. 42–1468. The X-ray diffraction patterns for α-Al_2O_3/ PVA nanocomposite films are shown in Fig.1c. XRD patterns of all α-Al_2O_3/ PVA nanocomposite films showed a broad peak at 2θ≈19.90 which is attributed to PVA [19, 21] and the other peaks correspond to α-Al_2O_3. The diffraction peak correspond to α-Al_2O_3 is very small compared with that of PVA, because the concentration of α-Al_2O_3 is very low compared with that of PVA. This small peak increase by increasing α-Al_2O_3 contents reaching 15%, as shown in Fig.1c. Meanwhile, in the α-Al_2O_3/ PVA nanocomposite, the diffraction peaks of α-Al_2O_3 are fixed at 2θ and show diffraction patterns similar to those of pure α-Al_2O_3. This denotes that the α-Al_2O_3 unchanged after being doped into the PVA matrix. The mean crystallite size of the ordered α-Al_2O_3 nanoparticles has been inferred from Debye- Scherrer's formula [22]:

$$D = \frac{0.9\lambda}{\beta\cos\theta}$$

The estimated crystallite size of α-Al_2O_3 nanoparticles was found ≈ 29 nm.

3.2. FTIR analysis

The IR spectroscopy in the range 400- 1000 cm^{-1} can be utilized as a swift and easy gadget to characterize the entity of transition α-Al_2O_3 phase. The FTIR spectra for pure PVA, α-Al_2O_3 / PVA nanocomposite films and α-Al_2O_3 are shown in Fig. 2 (a-c). In the spectra of pure PVA and α-Al_2O_3 / PVA nanocomposites, the broad and strong band posted at 3340 cm^{-1} which assigned to the stretching vibration of hydroxyl group (OH) [23]. The

robust band at 2940 cm^{-1} is attributed to the band of asymmetric CH stretching [24]. The two bands recognized at 1712 and 1658 cm^{-1} are assigned to the stretching vibrational band of C=O [25]. The two bands spotted at

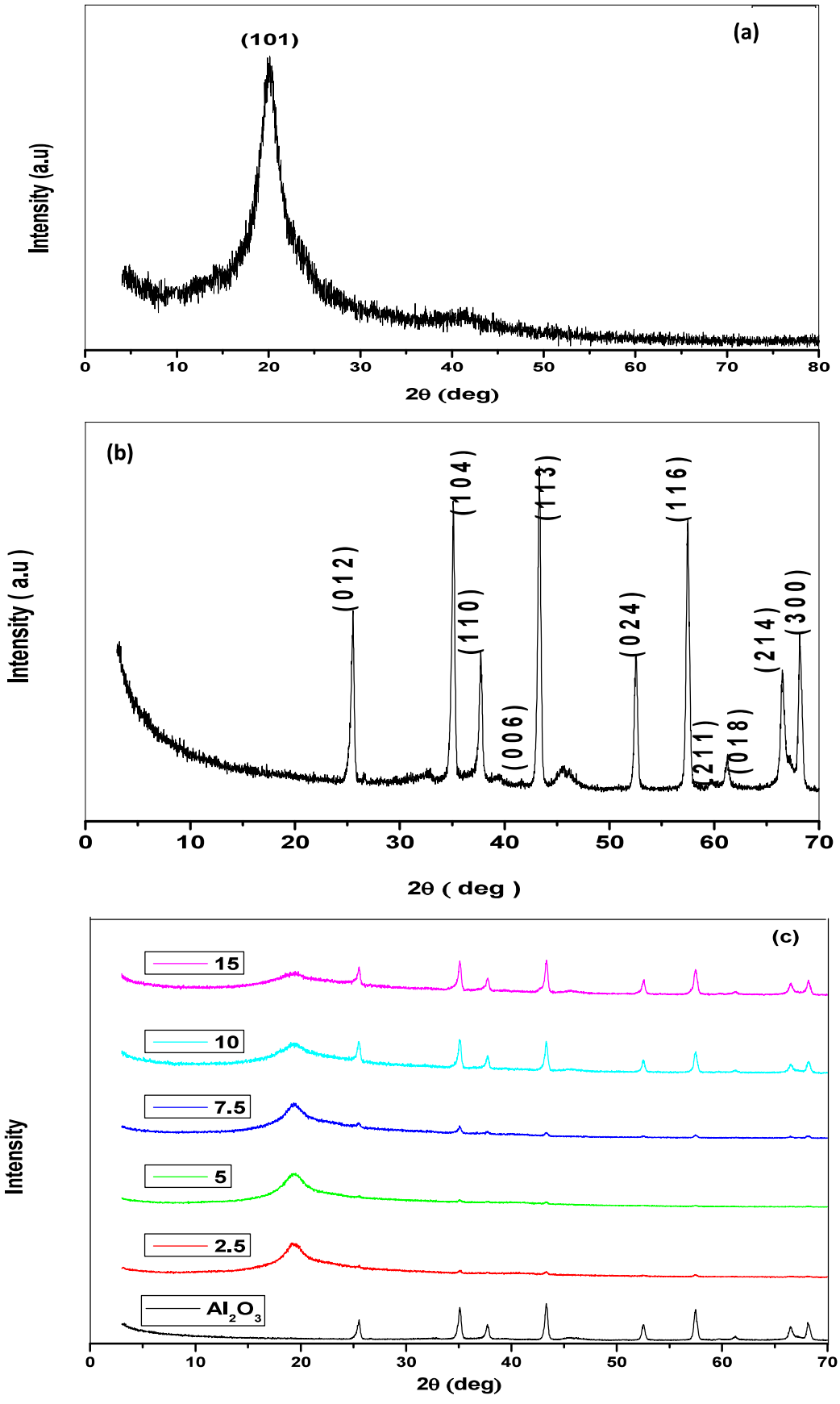

Fig. 1(a-c): XRD pattern of pure PVA, α-Al_2O_3, α-Al_2O_3/ PVA nanocomposite films.

1427 and 1330 cm^{-1} are indexed as CH_3 bending vibration and CH_2 stretching, respectively [26]. The band at 1090 cm^{-1} engenders from the C–O stretching vibration while the band at 920 cm^{-1} generates from CH_2 rocking vibration [27]. Also, the band at 850 cm^{-1} rises from C–C stretching vibration and that at 660 cm^{-1} arises from out of plane OH bending [19, 28]. The coalition α-Al_2O_3 NPs in PVA produced slight mutates in the intensities of absorption bands besides the production of new absorption bands in the range of 600–400 cm^{-1}; attributed to the Al–O stretching. This result assured the entity of α-Al_2O_3 NPs in the PVA matrix. By adding 2.5 % and 5.0% Al_2O_3, the bands were shifted higher wavenumber to 3575 and 6515 cm^{-1}, respectively attributed to the Al–O stretching.

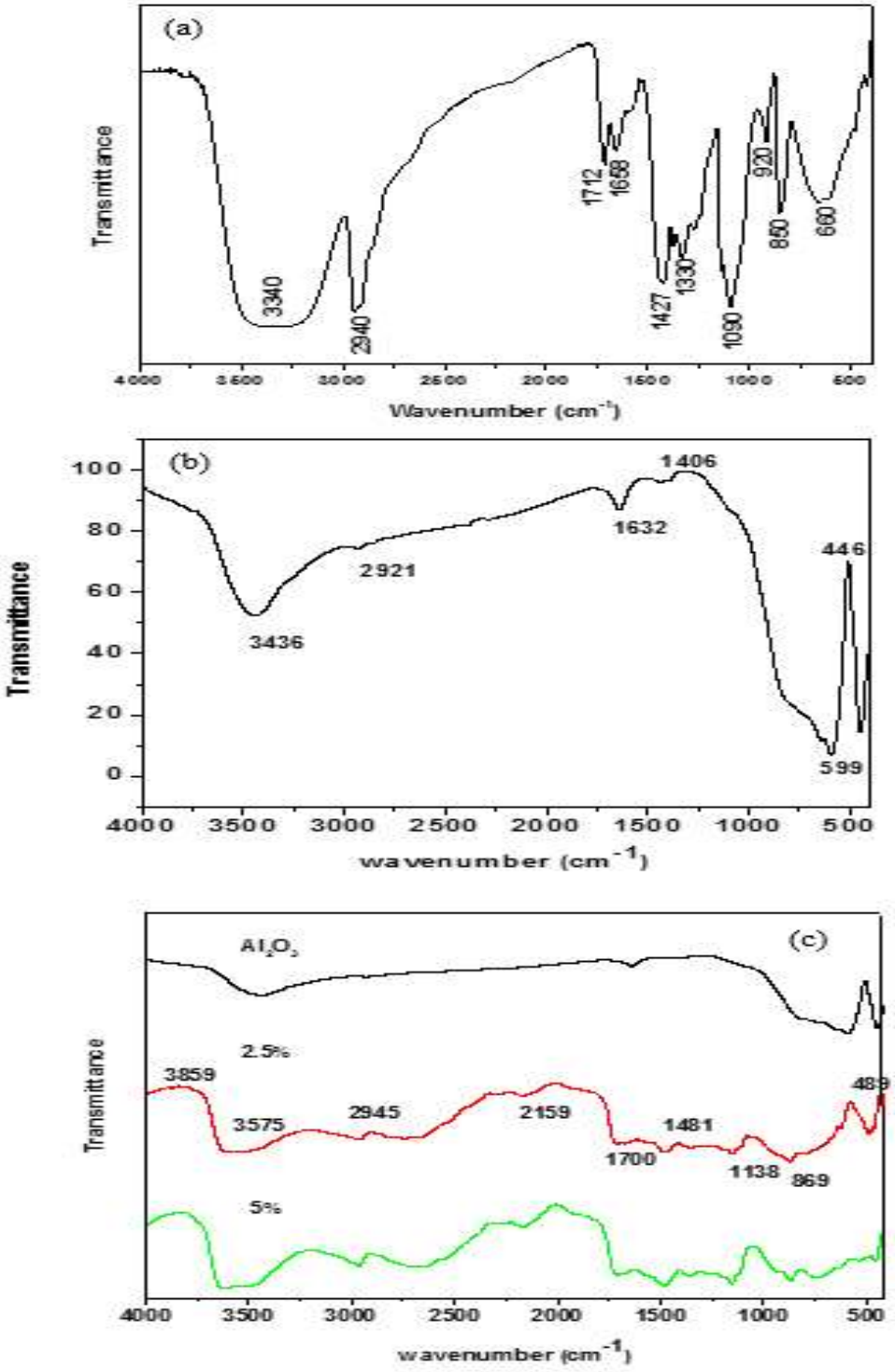

Fig. 2(a-c): FTIR spectrum of of pure PVA, α-Al_2O_3, α-Al_2O_3/ PVA nanocomposite films.

3.3. Electron microscopy analysis

HRTEM micrographs of α-Al_2O_3 nanoparticles are illustrated in Fig. 3a which exhibit clear platelet shape of hexagonal form, with average size 10 nm. Fig. 4(a,b) illustrates the field emission scanning electron micrographs FESEM images of α-Al_2O_3/PVA of 2.5% and 5% wt. nanocomposite, where it looks like clusters of cauliflower shape. From these micrographs, it was demonstrated that α-Al_2O_3 NPs were dispersed in the PVA matrix, because the α-Al_2O_3 nanofiller having excellent adhesion and strong interfacial bonding to the PVA beads. In addition, the results exihibited that the structure of the prepared 5% Al_2O_3 was more uniform than that of 2.5% Al_2O_3. The EDX patterns of 2.5% and 5% wt. nanocomposites are presented in Fig. 5 (a,b). It is distinctly seen that the two above concentration consists of Al, C and O. The results indicate that the nanocomposite consists only of two phases namely α-$Al_2O_3$and PVA as well as no other phases was detected which assure its successful preparation.

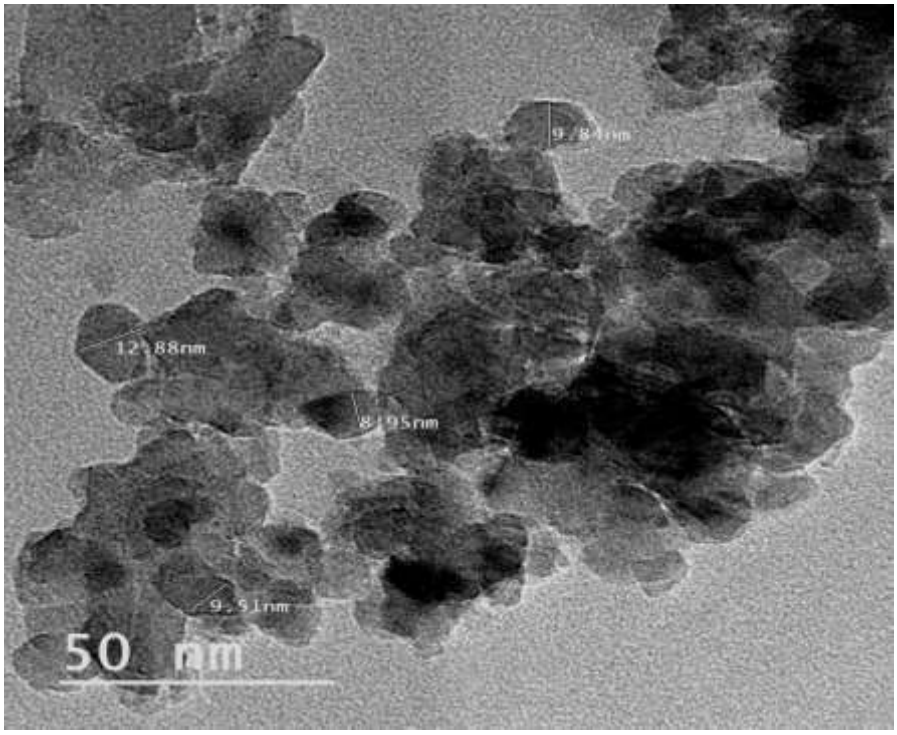

Fig. 3: HRTEM micrograph of the as-prepared α-Al_2O_3 nanoparticles.

3.4 Optical properties:

Fig. 6 (a-c) shows the optical absorbance transmittance and reflectance spectra as a function of the wavelength of the incident light for α-Al_2O_3/ PVA nano composites of various filler contents are. The figure manifests that, the absorbance increases as a result of filler addition but no shift in the peak position. The adding of different amounts of filler to PVA does not alter the chemical structure of the material but new physical mixture is established. The analysis of the absorption coefficient, α at the fundament absorption edge was found to follow the relation [29]:

$$\alpha h\nu = B(h\nu - E_{op})^n$$

Where B is a constant rely on the transition probability and the exponent n, is an index that characterizes the

optical absorption process and is theoretically equal (n =1/2) for a direct allowed transition, (n =3/2) for a direct forbidden transition, (n =2) for an indirect allowed transition and (n =3) for an indirect forbidden transition. α is the absorption coefficient, which calculated using the Beer- Lambert's relation [30]

$$\alpha = 2.303 \frac{A}{t}$$

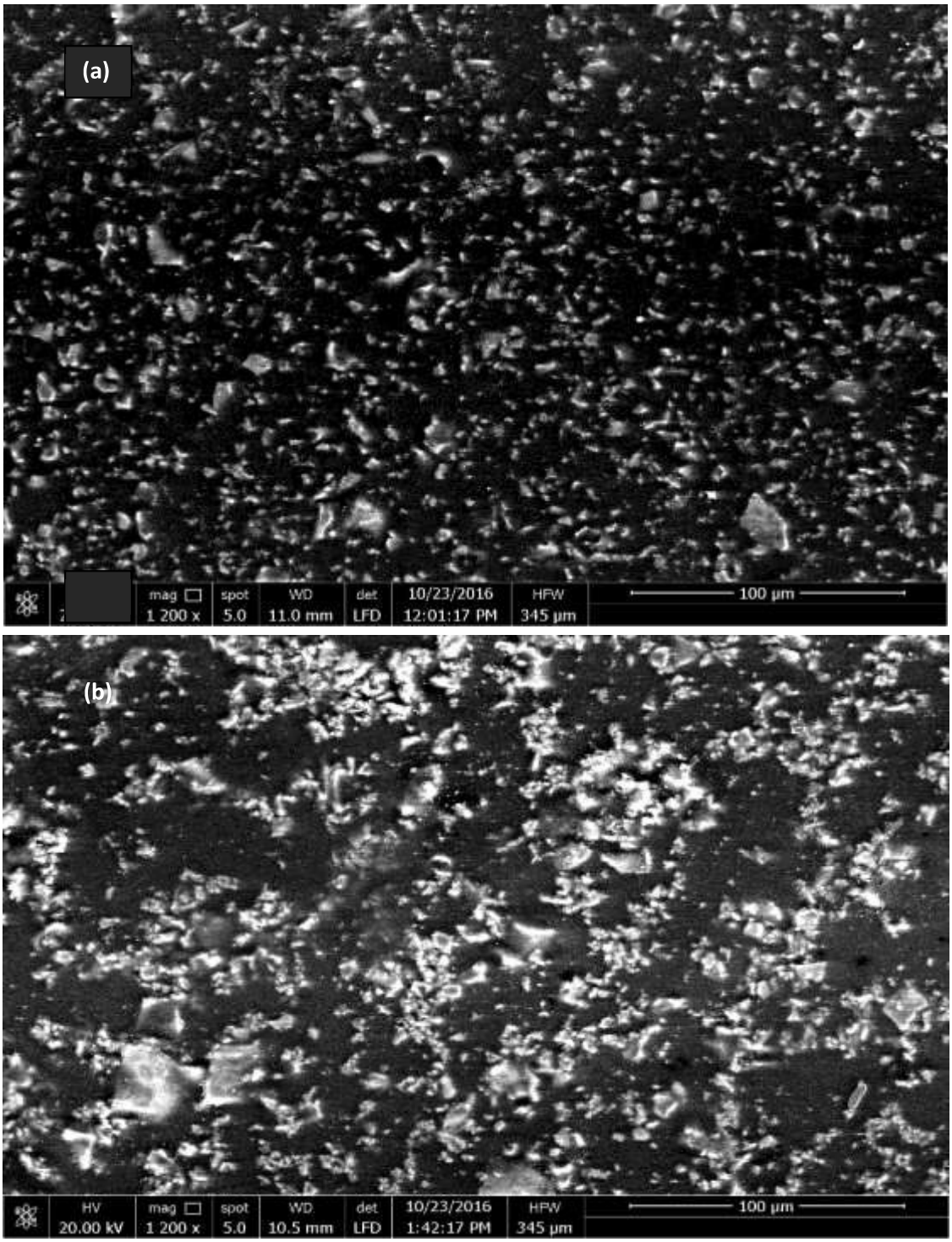

Fig. 4(a,b): FESEM micrograph of 2.5 and 5% α-Al_2O_3/ PVA nanocomposites.

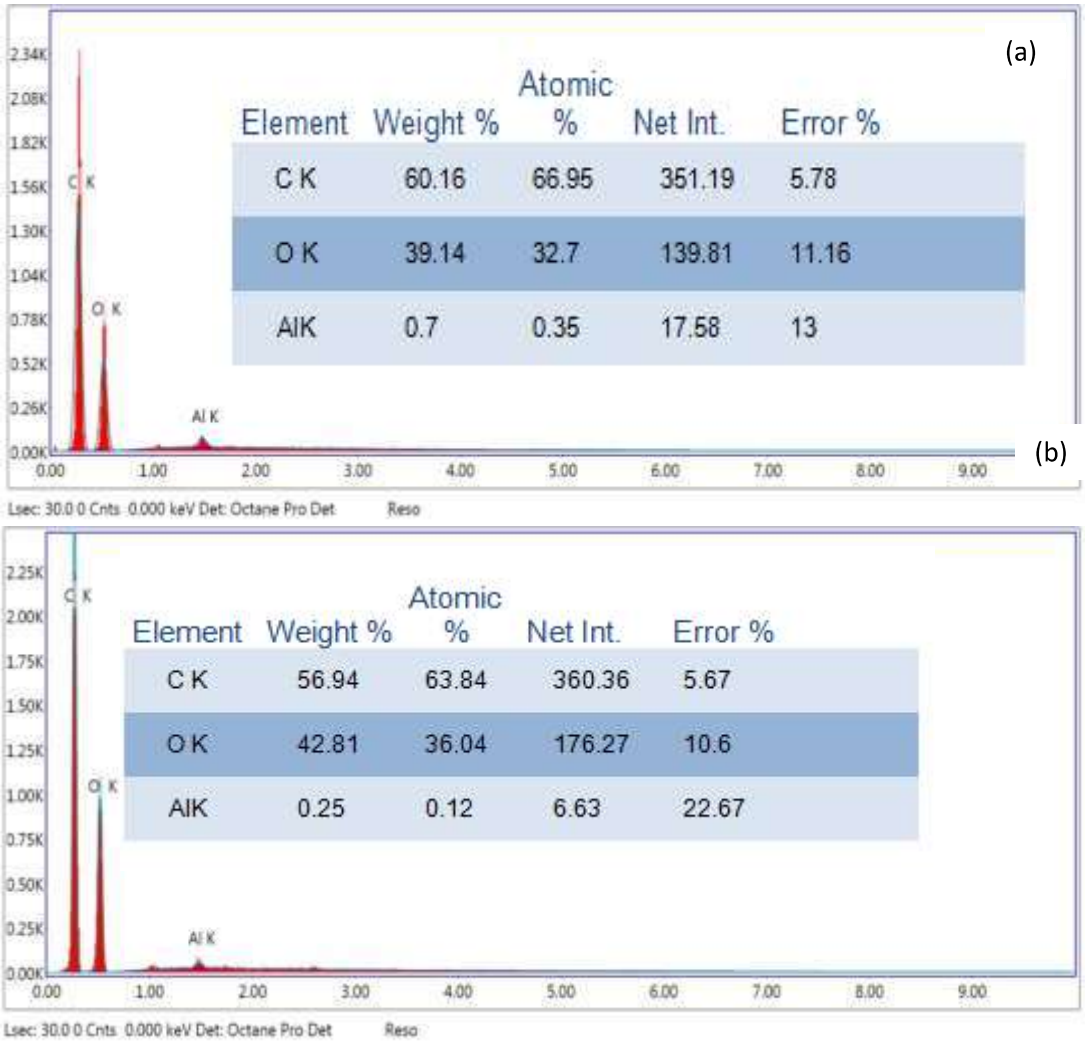

Fig. 5(a,b): EDS spectrum of 2.5 and 5% α-Al_2O_3/ PVA nanocomposites.

A and t are the absorbance and the thickness of the film. B is the parameter that depends on the inter band transition probability, hν is the incident photon energy, E_{op} is the optical band gap. Fig.7 shows the relation between absorption edges $(\alpha h\nu)^2$ for PVA and α-Al_2O_3/ PVA nanocomposites as a function of photon energy (hν), where n=1/2 for direct allowed. At extension of the curve to the value $(\alpha h\nu)^2 = 0$, we can determine the direct band gap of the composites. The conclude values of optical band gap of the PVA and composites are recorded in table 1. It is exhibited that;Pr the values of energy gap decrease with increasing α-Al_2O_3 concentration.

Table 1: Dispersion parameters of α-Al_2O_3/ PVA nanocomposite films at different concentration of α-Al_2O_3.

α-Al_2O_3%	E_g (eV)	E_o(eV)	E_d (eV)	E_o/ E_g	n_o	ε_s
0.0%	3.82	5.10	3.86	1.34	1.33	1.76
2.5%	2.99	4.85	14.80	1.62	2.01	4.05
5.0%	2.94	4.65	25.49	1.58	2.54	6.48
7.5%	2.75	4.37	36.67	1.58	3.06	9.39
10.0%	2.42	4.31	144.92	1.78	5.88	34.62
15.0%	2.33	4.14	366.37	1.79	9.46	89.49

The ultimate remarkable optical property is the refractive index (n). The refractive index depends on the wavelength of light, and this dependence is called dispersion. In The refractive index as a function of wavelength can be estimated from the reflection coefficient data R and the extinction coefficient k using equations [31- 32]:

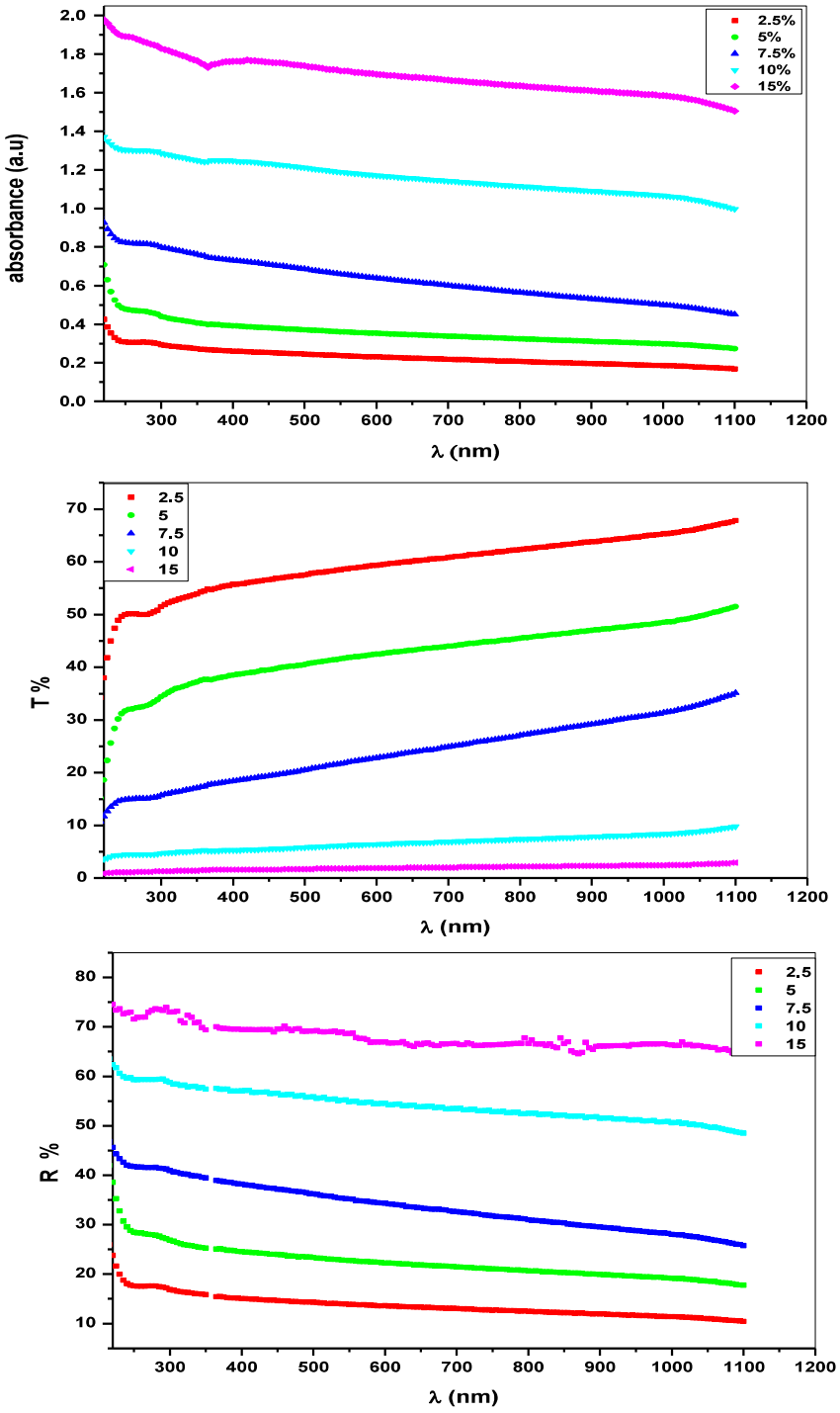

Fig. 6(a-c): UV-visible absorption, transmission and reflection spectra of α-Al_2O_3/ PVA nanocomposite films.

The ultimate remarkable optical property is the refractive index (n). The refractive index depends on the wavelength of light, and this dependence is called dispersion. In The refractive index as a function of wavelength can be estimated from the reflection coefficient data R and the extinction coefficient k using equations [31- 32]:

$$k = \frac{\alpha\lambda}{4\pi} \qquad n = \frac{(1+R)}{(1-R)} + \sqrt{\frac{4R}{(R-1)^2} - k^2}$$

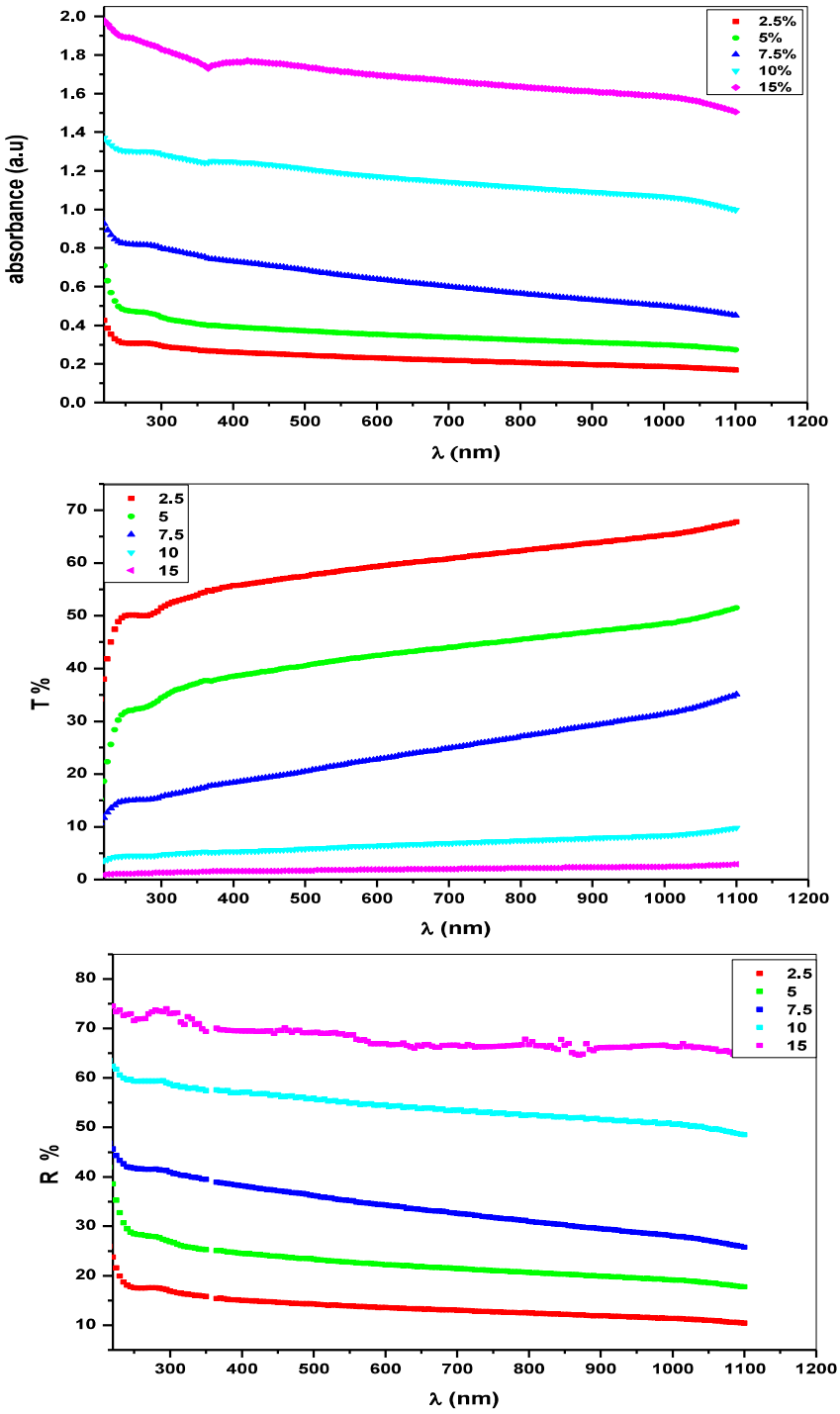

Fig. 6(a-c): UV-visible absorption, transmission and reflection spectra of α-Al_2O_3/ PVA nanocomposite films.

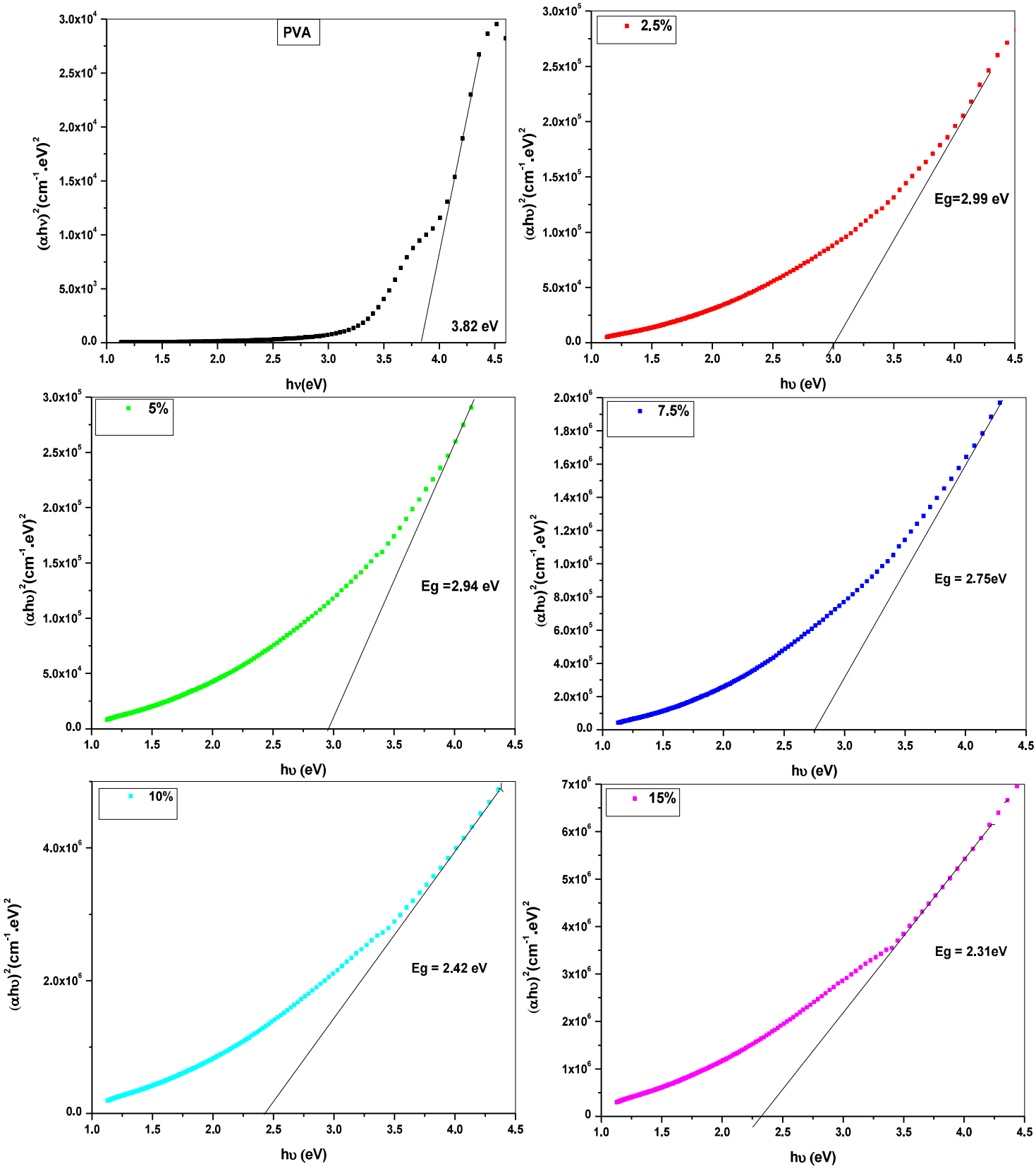

Fig. 7 Relation between $(\alpha h\nu)^2$ and $(h\nu)$ for the pure PVA and α-Al_2O_3/ PVA nanocomposite films.

Fig. 8 shows the variations of extinction coefficient with wavelength of α-Al_2O_3/ PVA nanocomposite. Fig. 9 shows the refractive index of the α-Al_2O_3/ PVA. The enhancement of the refractive index n and extinction coefficient k with wavelengths is correlated to the higher concentration of α-Al_2O_3 (from 25 to 15 wt. %) and thus more scattering of photons are occurred with the added aluminum oxide (α-Al_2O_3). The figure displays an increase with increasing fillers. The demeanor of (k) can be ascribed to high absorption coefficient. This result manifests that; the α-Al_2O_3 nanoparticles will amend the properties of the host polymer.

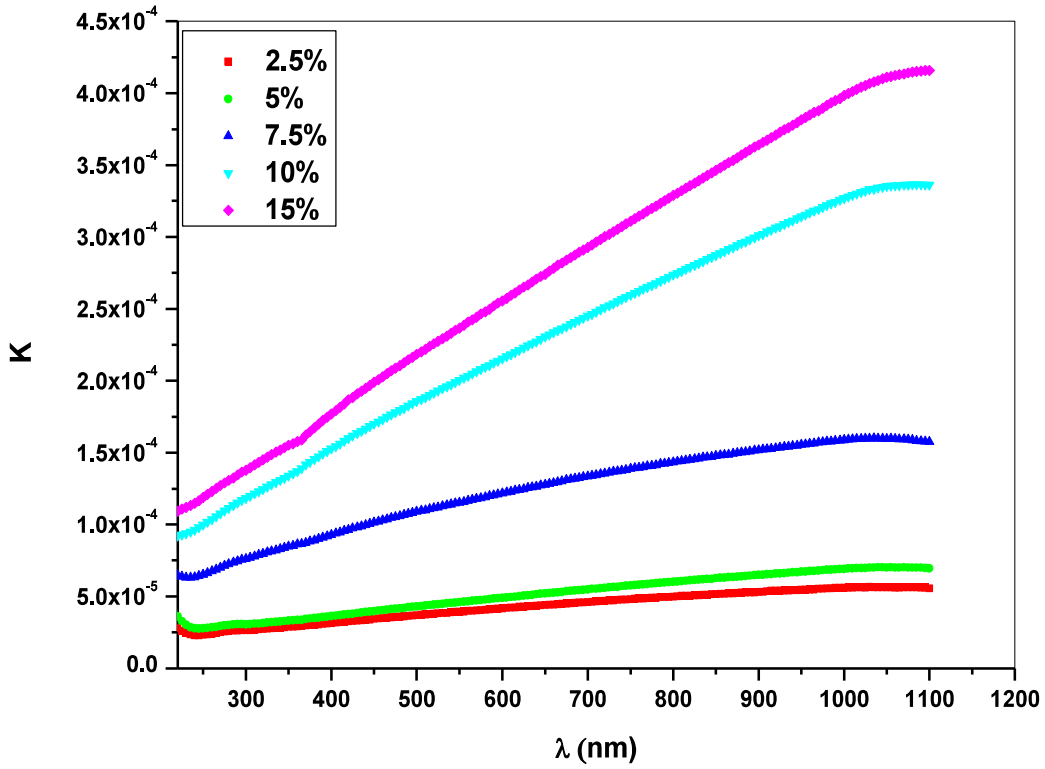

Fig. 8: The extinction coefficient of α-Al_2O_3/ PVA nanocomposite films.

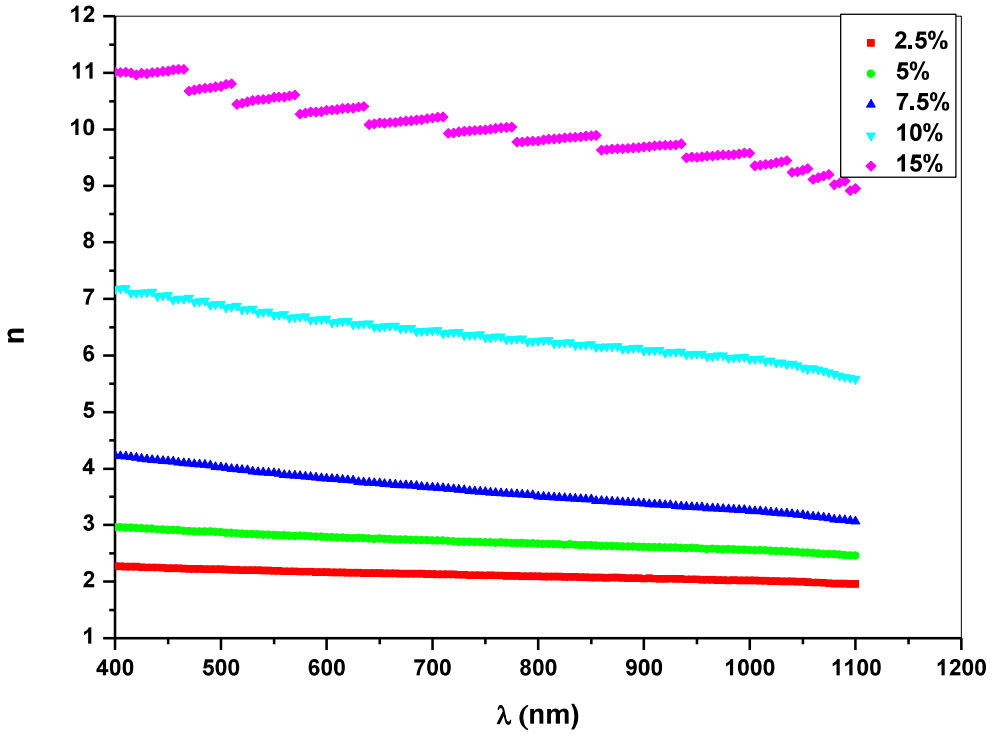

Fig. 9: The refractive index of α-Al_2O_3/ PVA nanocomposite films.

The energy dependence of the refractive index for PVA and α-Al_2O_3/ PVA can be fitted by using the single oscillator model in the normal dispersion region developed by Wemple and DiDomenico [33] as:

$$n^2 - 1 = \frac{E_o E_d}{E_o^2 - (h\nu)^2}$$

where E_o is the energy of the effective dispersion oscillator and E_d is the dispersion energy or oscillator strength. Fig. 10 illustrates $(n^2 - 1)^{-1}$ as a function of $(h\nu)^2$, for the investigated sample. E_o and E_d are obtained from the slope $(E_oE_d)^{-1}$ and intercept E_o/E_d. The static refractive index, n_o, at zero photon energy (long wavelength) can be predestined from equation, i.e $n_o^2 = 1 + E_d/E_o$, and then the static dielectric constant $\boldsymbol{\varepsilon_s}$ is given as $\varepsilon_s = n_o^2$. The values of E_o and E_d are listed in table 1. The oscillator energy, E_o is an "average" energy gap and, in close approximation, it scales with the optical band gap, E_g: $E_o \approx 2\ E_g$, as was found by Tanaka [34]. The ratio E_o / E_g for PVA and α-Al_2O_3/ PVA shows good agreement with this relation.

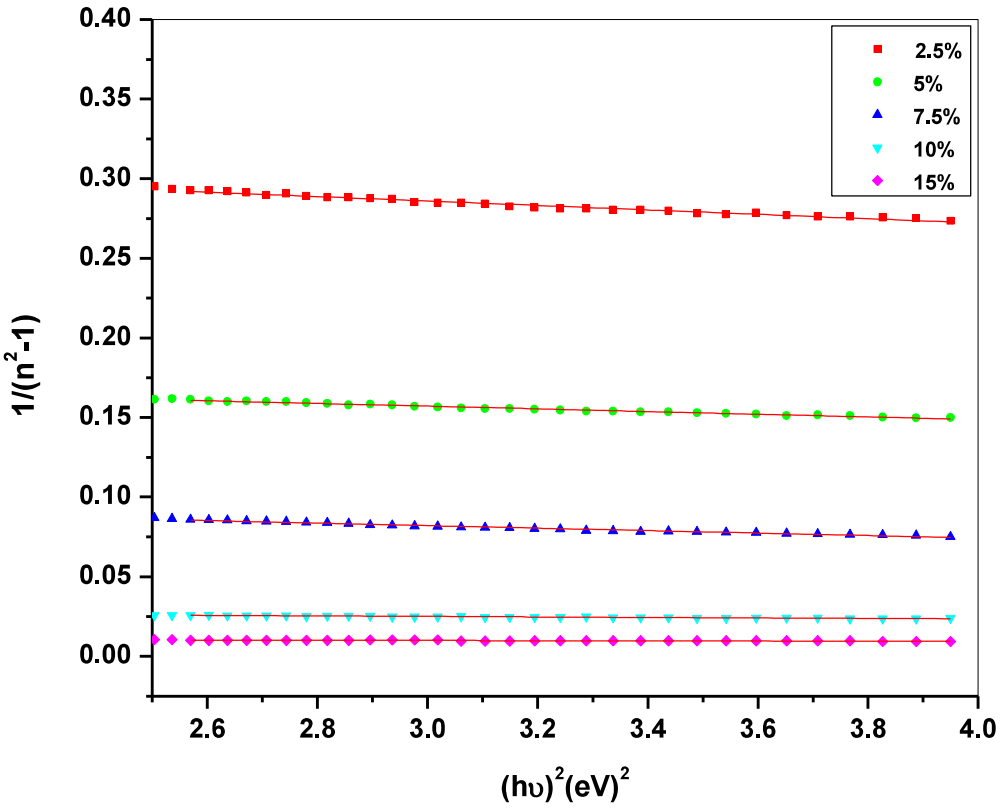

Fig. 10: Relation between$1/(n^2 - 1)$ and $(h\nu)^2$for α-Al_2O_3/ PVA nanocomposites.

3.5 Dielectric properties

Dielectric constant ε' of materials is fundamentally depends on sundry factors such as micro-structural arrangement, charge polarization and other agents [35].The real part of dielectric constant ε', has been estimated utilizing the following equation [36]:

$$\varepsilon' = \frac{c_p \times t}{\varepsilon_o A}$$

where c_p is the capacitance of the film in (F), ε_o is the permittivity of the free space (8.85×10^{-12} F/m), t is the thickness of film and A is the cross sectional area of the surface of the film. Dielectric loss ε'', has been determined using the following relation [36]:

$$\varepsilon'' = \varepsilon' tan\delta$$

The ac electrical conductivity σ_{ac}, of samples was evaluated by the relation [37]:

$$\sigma_{ac} = 2\pi f \varepsilon' \varepsilon_o tan\delta$$

where f is the frequency of the applied field and tanδ is the dielectric loss tangent.

Fig. 11(a-c) and Fig. 12(a-c) show the temperature dependence of dielectric constant ε' and dielectric loss ε'', for pure PVA and PVA/ α-Al_2O_3 nanocomposites in the frequency range 10 kHz- 5 MHz. All samples have possessed the same demeanor. Firstly, it is noticed that the dielectric constant ε' and dielectric loss increase ε'' increases with temperature but decreases with increasing frequency, i.e., ε' and ε'' have higher values in low frequency range and then decrease with increasing frequency. In low frequency range, besides polarization due to PVA and α-Al_2O_3, the space charge polarization plays a major role in increasing dielectric constant of composite [38]. The space charge polarization arises from the α-Al_2O_3/PVA interfaces. The dielectric constant increases with weight fraction of α-Al_2O_3. The increase in dielectric constant with weight fraction of α-Al_2O_3 upholding the fact of the space charges polarization contribution. The dielectric constant of composite increases with addition of α-Al_2O_3 reflects the formation of capacitance network of Al. [39].

Fig. 13(a-c) shows the relationship between the ln(σ) and inverted absolute temperature of the α-Al_2O_3/PVA nanocomposites. It is clear that the conductivity increases with increasing temperature. At low temperature region, the conductivity is slightly temperature and frequency dependent. In this region, the thermal energy is not appropriate to unleash charge carriers and increasing the frequency could reinforce their hopping. At high temperature region, the conductivity becomes frequency independent and a linear relation was obtained. The activation energy and conduction mechanism can be determined using equation $\sigma = \sigma_o exp(-E_a/k_BT)$ and tabulated in Table 2. The high activation energy values for neat sample and low α-Al_2O_3 concentration sample can be attributed to the thermal movement of the ions and molecules. Whereas the low activation energy values for the samples of higher α-Al_2O_3 content can be attributed to the electronic conduction mechanism which is related to the decreasing of the distance between the α-Al_2O_3 particles [39]. Furthermore, it was observed that values of the activation energies in eV for pure PVA, α-Al_2O_3/ PVA nanocomposites decreased with increasing frequency. The composition dependence (α-Al_2O_3) of ε′, tan δ and σ_{ac} at (10 kHz and 303 K) are given in Fig.14 (a-c).

Table 2: Values of the activation energies in eV for pure PVA, α-Al_2O_3/ PVA nanocomposites at different frequencies.

f (Hz)	PVA	2.5 %	5.0 %	7.5%	10.0 %	15.0 %
10000	0.33	0.76495	0.63429	0.66488	0.790	0.85373
100000	0.25	0.75101	0.53684	0.79162	0.780	0.71108
1E6	0.14	0.67002	0.48099	0.5338	0.480	0.27921
3E6	0.09	0.36814	0.29538	0.23351	0.199	0.08293

5E6	0.07	0.23349	0.15271	0.1049	0.086	0.04018

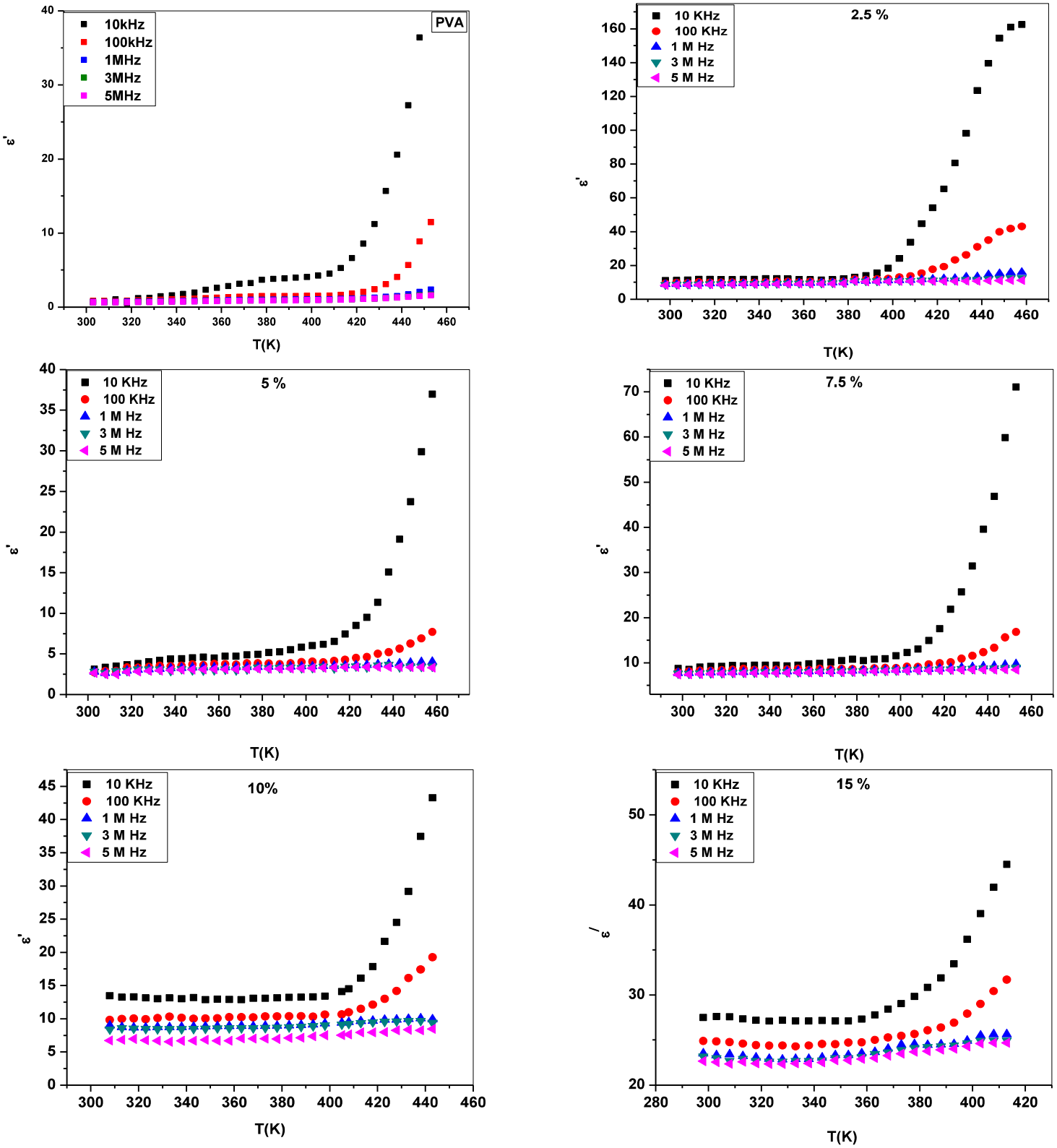

Fig. 11: Dependence of dielectric constant έ, on absolute temperature for pure PVA, αAl_2O_3/ PVA and pure αAl_2O_3 in the frequency range 10 kHz- 5 MHz.

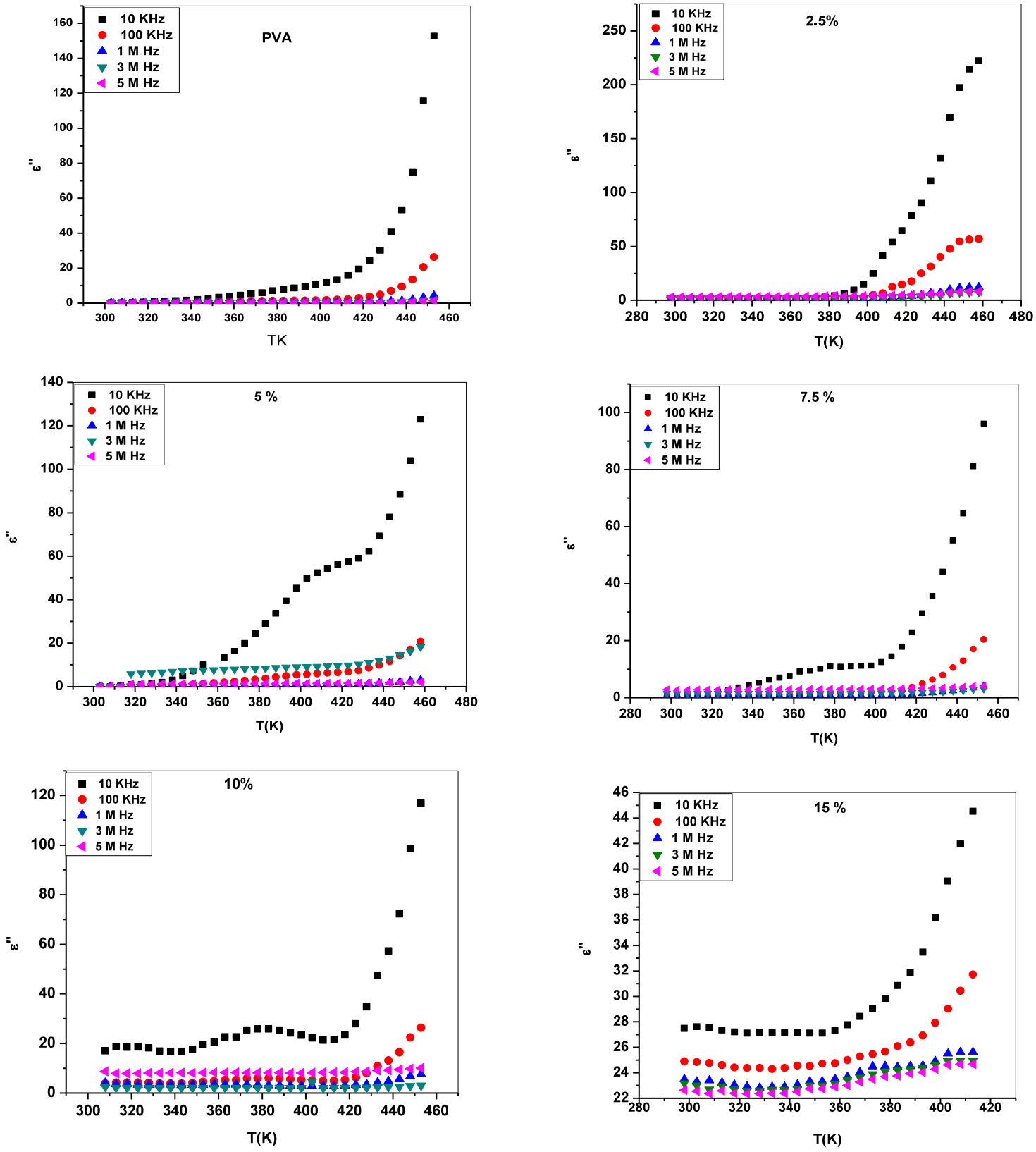

Fig. 12: Dependence of dielectric constant ε'', on absolute temperature for pure PVA, α-Al_2O_3/ PVA in the frequency range 10 kHz- 5 MHz range 10 kHz- 5 MHz.

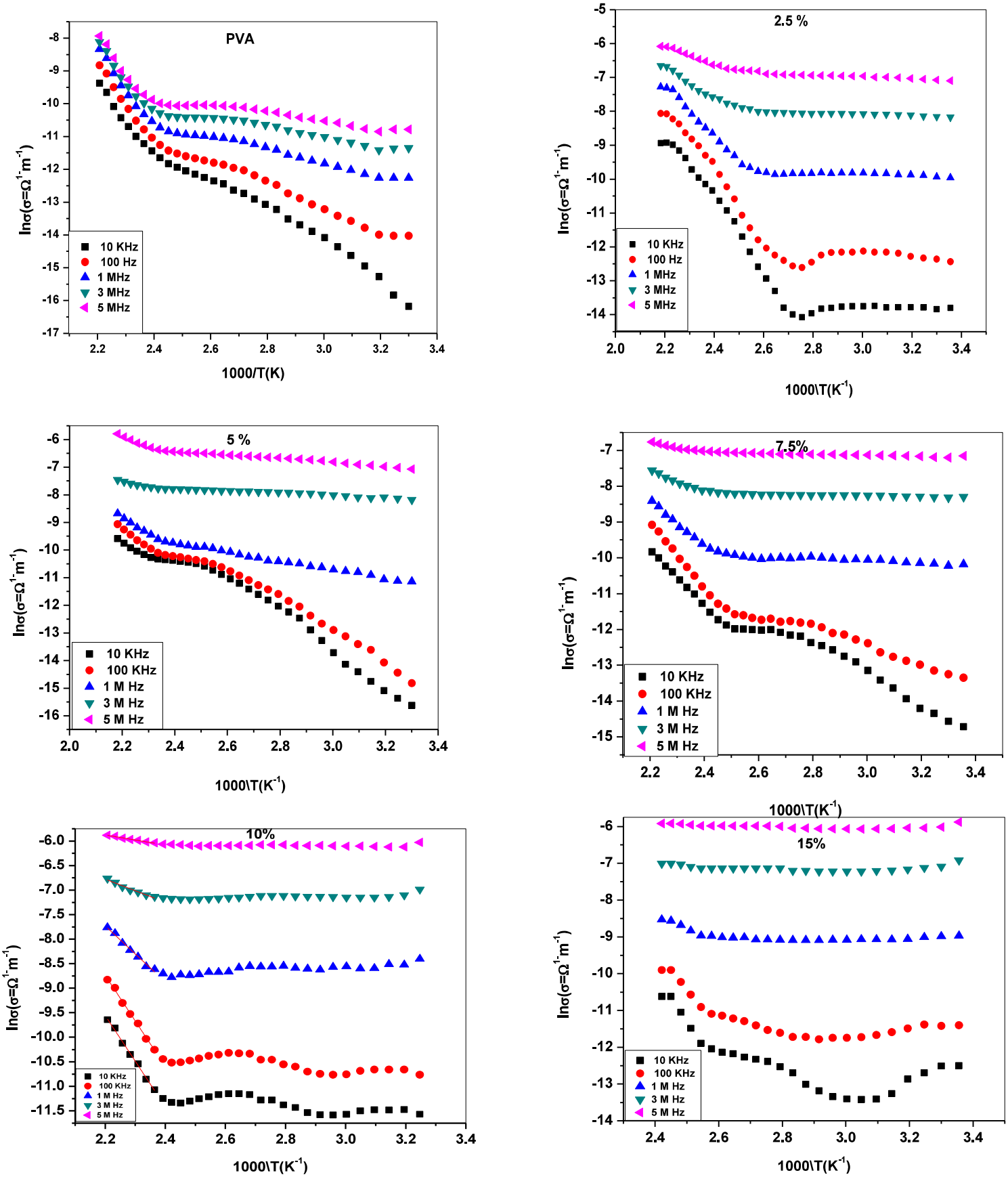

Fig. 13: Dependence of ac conductivity on the reciprocal of the absolute temperature for pure PVA, α-Al_2O_3/ PVA in the frequency range 10 kHz- 5 MHz.

It is clear that, ε′ and σ_{ac} have the same trend; they increase with α-Al_2O_3 content, till x=10 wt%, and then decrease. Tanδ at first increase with α-Al_2O_3 content, then decrease for x=10 wt%, and finally increase again. Thus the critical composition is PVA/ 10% α-Al_2O_3 which is a suitable nanocomposite for different applications. It was reported that the increase of the electrical conductivity is accompanied by an increase of the eddy current, which in turn increases the energy loss to tan δ. This behavior can be attributed to a gradual decrease in the series resistance with increasing frequency [40].

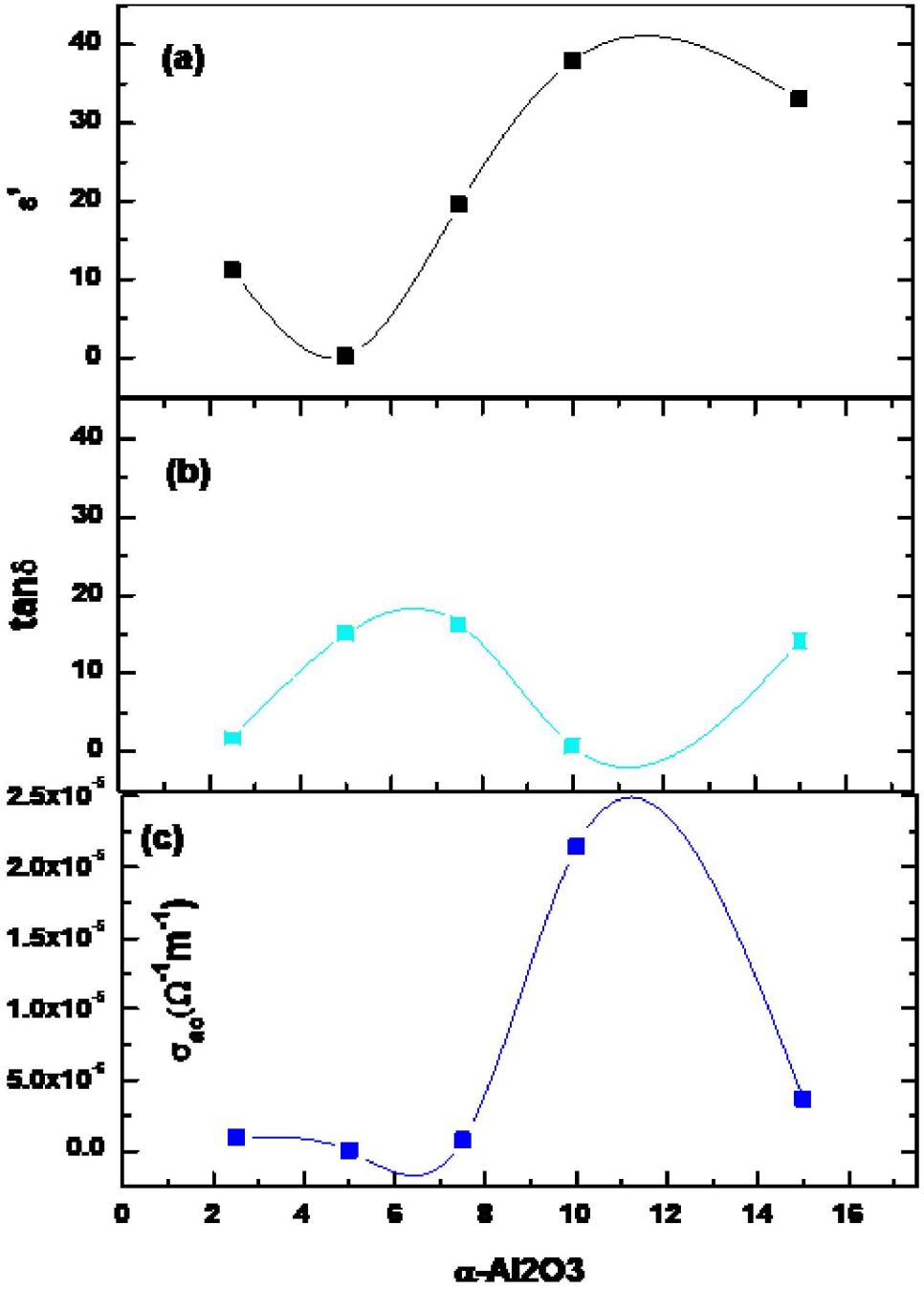

Fig. 14(a-c): The composition dependence of (a) ε', (b) tanδ and (c) σ_{ac} 10 kHz and 303 K.

4. Conclusion

Alumina ceramic nanoparticles were successfully prepared using the citrate-nitrate combustion method. XRD spectrum shows rhombohedral (hexagonal) structure of α-Al_2O_3. A series of PVA/ α-Al_2O_3 hybrid films was prepared by the casting method. XRD, FTIR, FE-SEM, EDS, and UV/Vis spectroscopy verified the formation of α-Al_2O_3 NPs and PVA/ α-Al_2O_3 NCs. The optical band gap is found to decrease with increasing Al_2O_3 NPs content from 3.82 eV to 2.33 eV. The nanocomposite with concentration (10% wt) has the highest dielectric constant, lowest dielectric loss and highest electrical conductivity. The properties of virgin PVA is modified and improved by doping with α-Al_2O_3 NPs, making it a promising material for different applications.

Conflicts of Interest

The authors declare that they have no conflicts of interest.

References

1. W. Ueda, M. Sadakane, H. Ogihara, Catal. Tod. 132, 2 (2008).
2. T. Gessner, K. Gottfried, R. Hoffmann et al., Micro.Techn. 6, 169 (2000).
3. J. H. Kim, E. K. Kim, C. H. Lee, M. S. Song, Y.-H. Kim, Phys. E 26, 432 (2005).
4. P. D. Pria, Europ. J. Orth. Surg. Traum. 17, 253 (2007).
5. H. Farsi, F. Gobal, J. Sol. St. Electrochem. 11, 1085 (2007).
6. A. C. Dillon, A. H. Mahan, R. Deshpande, P. A. Parilla, K. M. Jones, S.-H. Lee, Thin Sol.Films 516, 794 (2008).
7. S. Mallakpour, M. Dinari, J. Reinf. Plas. Comp. 32(4), 217 (2013).
8. D. Yan, J. He, X. Li, L. Jianxin, Z. Huili Ding, Surf. Coat.Technol. 141 , 1(2001).
9. Y.-S. Chang, N. Roy, J. Vac. Sci. Technol. 7, 1303 (1989).
10. R.K. Nahar, V.K. Khanna, Sens. Actuators, Int. J. Electron. 52, 557 (1982).
11. F. Werner et al. Proc. 27, 319 (2012).
12. Miguel Henrique Borattoet, Mater. Res. 17 (6), 1420 (2014).
13. S. Thomas, Tayol and Francis Group, LLC (2010).
14. Y.W. Mai et al. Poly. nanocomposites (2006).
15. Sunil K Sahi, PhD, The University of Texas at Arlington (2016).
16. Tantis, G. C. Psarras, D. Tasis, Poly. Lett. 6, 283 (2012).
17. M. Farahmandjou, N. Golabiyan, Trans. Phenom. Nano Micro Scales 3(2), 100 (2015).
18. S. F. Mansour, M. A. Abdo, S. I. El-Dek, J. Mag. Mag. Mater. 422, 105 (2017).
19. K.S. Hemalatha, K. Rukmani, N. Suriyamurthy, B.M. Nagabhushana, Mater. Res. Bull. 51, 438 (2014).
20. P. Kunal, K.B. Ajit, K.M. Dipak, AAPS Pharm Sci.Tech. 8, 1 (2007).
21. R.C. Agarwal, et al. New J. Phys. 10, 43023 (2008).
22. B.D. Cullity, Elements of X-ray Diffraction, Reading, MA, (1978).
23. X. Yuan., Polym. Bull. 67, 1785 (2011).
24. A. S. Roy, S. Gupta, S. Sidhu, A. Parveen, P. C. Ramamurthy, Comp.: part B 47, 314 (2013).
25. S Gunassekaran, E Sailatha, S Sesshadri, S Kumaresan, Ind. J. Pure Appl. Phys. 47, 12 (2009).

26. S. Keskin, U. Ibrahim, T. Tunc, M. Öztür, A. Aytimur, Mater. Manuf. Proc. 26, 1346 (2011).
27. Z. Ali, H. Youssef, T. Afify, Polym. Comp. 105, 2976 (2007).
28. P.I. Devi, K. Ramachandran, J. Exp. Nanosci. 6, 281 (2011).
29. J.I Pankove., Optical Processes in Semiconductors, Prentice-Hall, New Jersey (1971).
30. A.F. Mansour, S.F. Mansour, M. A. Abdo, IOSR J. Appl. Phys. 7, 60 (2015).
31. Hussain A. Badran, Amer. J. Appl. Sci. 9, 250 (2012).
32. I. S. Yahia, A. A. M. Farag, M. Cavas, F. Yakuphanoglu, Super lattice. Microst. 53, 63 (2013).
33. S. H Wemple, M DiDomenico Jr., Phys. Rev. B 3, 1338 (1971).
34. K. Tanaka, Thin Solid Films 66, 271 (1980).
35. P. S. Das, G. P. Singh, J. Mag. Mag. Mater. 401, 918 (2016).
36. S.F. Mansour, M.A. Abdo, J. Mag. Mag. Mater. 428, 300 (2017).
37. S. Demirezezn, Appl. Phys. A 112, 827 (2013).
38. M. Hamzah, E. Saion, A. Kassim, E. Mahmud, I. Shahrim, J. advance. sci. 1, 9 (2009).
39. M. Hamzah , E. Saion, A. Kassim, M. Yousuf, MPJ. 3, 24 (2008).
40. D. E. Yıldız, İ. Dökme, J Appl Phys. 110 (1)14507 (2011).